A Review of Signal Processing and Analysis

Max Lee *
Lab Partners: Basil Kyriacou, Connor McWard , James Mang

Department of Astronomy, University of California, Berkeley

February 11, 2020

Abstract

We present a review of basic signal processing and analysis. We find strong evidence for the Nyquist Criterion existing at a frequency of $\nu_{sample}/2$, as well as the frequency resolution of discrete Fourier transforms to be at, ν_{sample}/N. We develop a framework for analyzing data in a frequency domain and use this to experiment with windowing functions and spectral leakage. We show evidence for the correlation theorem and convolution theorem in analysis of noise samples, windowing functions and side-band mixers.

1 Introduction

The goal of this work is to provide an overview of basic signal processing while verifying essential theorems experimentally. Much of our work consists of describing how to properly capture a signal so that analysis can be accurately performed. Through this analysis we develop an understanding of how radio frequency observations are inferred and worked with.

We begin, in section 2, discussing the methods used to obtain our data by explaining equipment, code, technical issues we faced and possible sources of error. We then provide an analysis on signal processing basics in section 3. We present experimental evidence for the Nyquist Criterion which leads into a discussion on Discrete Fourier Transforms and representing our data in a frequency domain. This allows us to explore frequency windowing and resolution as well as the significance of 'negative frequencies' and complex signals. With the theoretical background from this discussion we then explain the convolution and correlation theorem through the scope of spectral leakage and windowing functions. We then consider how our analysis can be applied with examples of noise averaging and frequency mixing in section 4. We conclude with a recapitulation of the main concepts, highlight the gaps in our knowledge, and provide ideas for future works.

2 Methods

2.1 Equipment and code

Digitally sampling an ideal sine wave involves a minimum of two physical components: A function generator and a analog to digital converter (ADC). The first is used to create an approximately infinite sine wave with mutable frequency and amplitude, while the latter is used to take snapshots of voltage, converting it into binary code. In this work we use the 16-bit analog to digital converter, *PicoSampler 2000* and associated python module *ugradio.pico*[1]. The PicoSampler 2000 has the ability to take 'snapshots' at a frequency of $62.5\,MHz/N$, where N is an integer value. With each snapshot, the sampler finds the bit with the closest corresponding voltage and sends that value in binary to the user through *ugradio.pico*.

*maxlee1993@berkeley.edu

[1] `https://github.com/AaronParsons/ugradio/tree/master/ugradio_code`

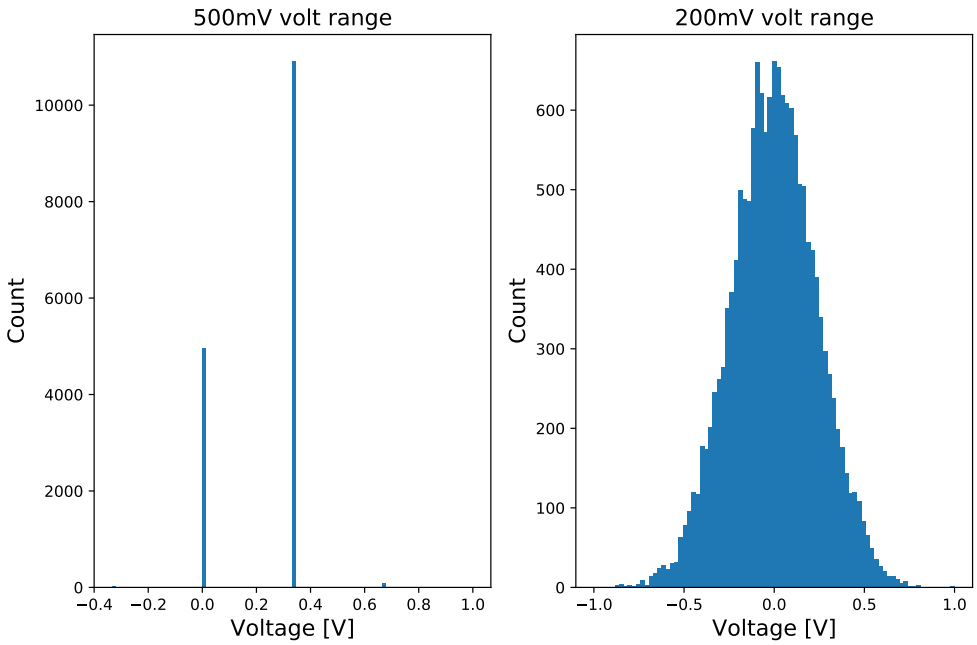

Figure 1: When sampling in the wrong volt range, the PicoSampler will round data to the nearest bit providing an inaccurate measure of data. Here we show a histogram of Gaussian noise sampled at too high of a volt range in the *Left Plot* causing the signal to appear in only 3 bins of voltage, and the same signal propperly sampled in the *Right Plot* showing the gaussian shape in voltage that we would expect

We additionally utilize a noise generator and ZAD-1 mixers in section 4. This provides samples of random Gaussian noise and signal multiplication respectively.

The output of the PicoSampler can be deceptive if wrongly parameterized. If the spread in voltages from the function generator is too great for the requested spread in bits, the sampler will return the highest voltage for consecutive readings resulting in a 'clipped' signal. The opposite case is when the signal from the function generator has too small of a voltage range when compared to the spread in bits. This has the effect of causing pairs, or a series, of consecutive readings to have the same bit value due to rounding.

This implies that the correct use of the volt range is crucial for accurate measurements, and we found that a range closest to the peak to peak voltage provided the most accurate result. In figure 1 we show a sampling of Gaussian noise with an amplitude of $V_{pp} = 120\,mV$, highlighting the effect of sampling at too high a volt range, $V_{samplerange} = 500\,mV$. When compared to $V_{samplerange} = 200\,mV$ we see that our signal represented a Gaussian as opposed to two voltage bins.

While packages such as *ugradio.dft* for Fourier transforms and *numpy.correlate* for correlation functions are available, we find that that the *numpy.fft* module contains an accurate, and fast, discrete Fourier transform. As illustrated in section 3, the power spectrum and auto-correlation functions can both be determined using *numpy.fft*. Similarly, we found that the manually computed auto-correlation function conserves power more effectively then *numpy.correlate*.

2.2 Sampling Rate and Sources of Error

We use a sampling rate of $\nu_s = 31.25\,MHz$, and input amplitude of $V = 0\,dBm$ for all of our samples unless otherwise noted. Using a subset of 300 samples we capture most of the necessary details in our data and conserve computational time. We utilize all 15800 viable samples in our discussions of noise, and analysis of mixers (section 4). The former requires averaging which is dependant on the number of samples and we wished to highlight this effect; while the later we opted for a higher frequency resolution in our power spectra.

This work discusses the Nyquist Criterion and naturally we sample above the Nyquist frequency to verify

its effect in section 3. Other than this verification, and a discussion on windowing in section 4, we only use data from frequencies inside of a bandwidth $[-v_s/2, v_s/2]$.

It is important to note that because of the quantized nature of the PicoSampler, it is impossible to fully reconscruct the original signal at full resolution. Just the fact that the sampler is not taking an (impossibly) infinite length of sample, misconstrues our data analysis as we will see in section 3. Further, through this work we were informed of a bug in the sampler rendering the first 200 samples of data inaccurate.

3 Data Analysis

We begin this section by explaining and testing the Nyquist Criterion through a comparison of ideal and sampled periods. We then discuss the power and voltage spectra of signals, emphasizing the effect of windowing and evidence of a finite frequency resolution. Following this, we explain the convolution and correlation theorems using spectral leakage as an application.

3.1 Sampling Theory and The Nyquist Criterion

When sampling, one can imagine a snapshot of some signal is taken at even time increments and later on, all the snapshots are patched together reconstructing the original signal. The rate at which these snapshots are taken is the sampling frequency (ν_s), and we wish to test the Nyquist Criterion. This would show the minimum ν_s necessary to accurately reconstruct a signal is twice the frequency of the input signal (ν_0). We write this as,

$$\nu_N = \nu_S/2 \tag{1}$$

Where ν_N is the Nyquist frequency and represents the maximum ν_0 allowable given a ν_s. The reason this is valid is that if we sample at less than the Nyquist Frequency we are taking less than 2 snapshots of our signal per wave. Consider taking a picture of a rotating carousel once per rotation. It would be impossible to resolve the direction or period of rotation for the carousel, just as in our case, it is impossible to resolve the period of the original wave and thus the frequency.

To test the validity of the Nyquist Criterion, we use a $v_S = 31.25\,MHz$, and capture consecutive signals increasing in integer multiples of $.1\nu_s$. We then calculate the average period of each sample expecting parallel values with the original signal up until $.6\nu_s$. We show in fig 2 that the error between our sampled and ideal periods is virtually none up until $.6\nu_s$. Following this the periods diverge and the error grows. It seems that our hypothesis was cogent and the Nyquist Criterion holds true.

The growth of the period past the Nyquist frequency in fig 2 is known as aliasing and describes the phenomena of measuring a larger period, or slower frequency, then the true signal. Interestingly, there appears to be a reflective symmetry about the Nyquist frequency $\nu_N = .5\nu_s$ in fig 2 such that the aliasing of the signals follows a pattern. The apparent symmetry of the reflection can be explained by the effect of frequency windowing and the periodic nature of our signals discussed below.

3.2 Fourier Transform and Discrete Fourier Transforms

To understand why there is an apparent reflection about the Nyquist frequency in fig: 2, we first convert our analysis from a time domain to a frequency domain. We can do this using the Fourier transform (FT), a mathematical tool allowing us to express any continuous function as an integral of complex sine waves. This change of basis switches our domain from time to frequency while preserving signal amplitude and allowing conversion back to the time domain through its inverse. The FT and its inverse (IFT) are defined as,

$$\begin{aligned} \widetilde{F}(\nu) &= \int_{-\infty}^{\infty} F(t) e^{-2\pi i \nu t} dt \\ F(\nu) &= \int_{-\infty}^{\infty} \tilde{F}(\nu) e^{-2\pi i \nu t} d\nu \end{aligned} \tag{2}$$

The tilde implies that we are now viewing our function in the frequency domain.

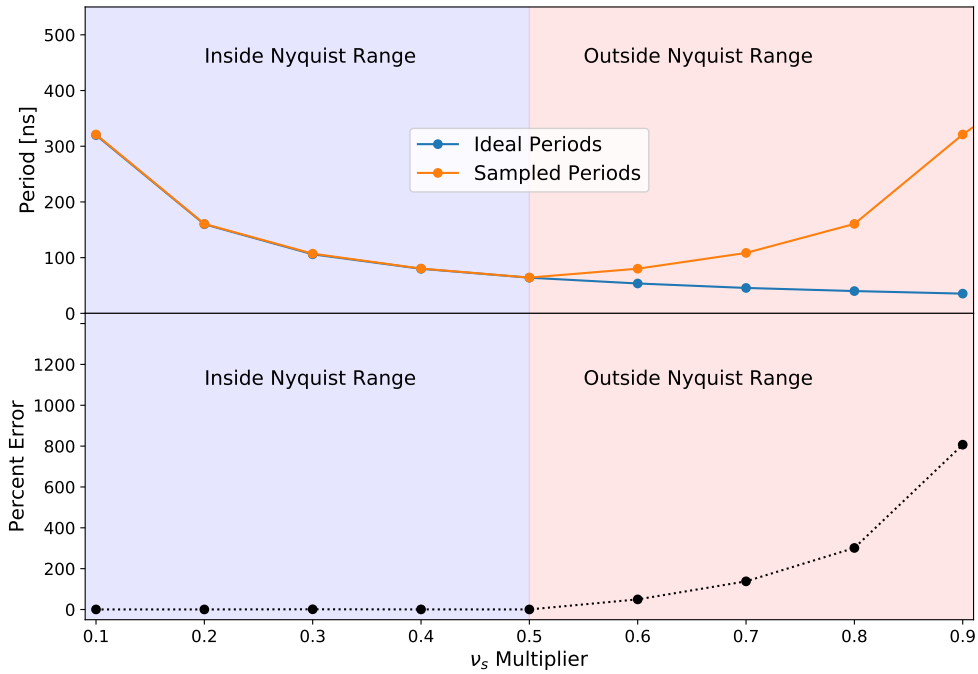

Figure 2: Here we show a sine wave can be sampled and reproduced such that the period and frequency match. But, this is contingent on the signal having frequency less than half that of the sampling rate. We plot the ideal periods (*Blue Dotted*) obtained from the measurement on the oscilloscope compared to the digitally sampled signal (*Orange Dotted*) for 9 different input signals which multiply our sampling rate (31.25MHz) by increasing multiples of .1. We show the zones considered inside the Nyquist criterion and greater than the Nyquist criterion (*Blue Shaded*, *Red Shaded* respectively) to emphasize where signals can be reproduced with confidence and where they cannot. Note the sharp delineation at $.5\nu_s$; exactly half the sampling rate. Further, we plot the percent error between the oscilloscope measurements and those obtained through sampling to show the discrepancies seen when sampling above the nyquist criterion.

The benefit to using Fourier transforms is we are able to uncover periodic fluctuations how much they dominate our signals. This can be represented in a power spectrum defined as,

$$P(\nu) = \widetilde{F}(\nu)\widetilde{F}^*(\nu) \tag{3}$$

Where the superscript $*$ refers to complex conjugate.

We are also able to extract both complex and real components from signals using a FT. These components represent the real parts and any phase information. This truth can be identified in Euler's identity,

$$\begin{aligned} e^{i\omega t} &= \cos(\omega t) + i\sin(\omega t) \\ e^{i(-\omega)t} &= \cos(\omega t) - i\sin(\omega t) \end{aligned} \tag{4}$$

where the negative frequency contains a phase shift of $pi/2$ in the complex plane. This means complex components are odd functions, anti-symetric about the complex axis, while real components are even functions and fully symmetric about the complex axis.

Unfortunately, to change to a frequency domain through a FT we must integrate an infinitely long signal over infinite time, which is... infinitely impossible. We work around this using the Discrete Fourier Transform (DFT), which takes the infinite integral and converts it to a discrete sum over samples. This reduces our job... infinitely... and is written as,

$$\tilde{F}(\nu) = \frac{1}{N}\sum_{n=0}^{N/2-1} F(n)e^{2\pi i\nu n/N} \tag{5}$$

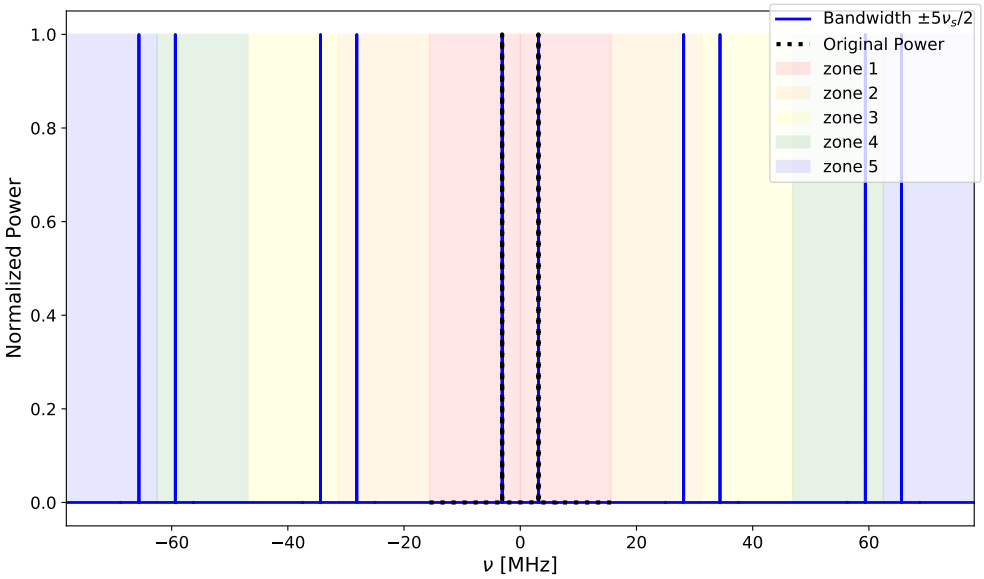

Figure 3: The effect of windowing as implied in fig 2, can be more explicitely seen in the frequency domain and by setting a bandwidth for frequencies larger than $[-\nu_N, \nu_N]$. Discrete Fourier transforming a non-aliased signal with this range symmetrically places the signal in neighboring zones reflecting about the integer multiples of the ν_N. Each zone is represented by a color of the rainbow, and for a signal DFT'd with a frequency bandwidth of $[-5\nu_N, 5\nu_N]$ (*Blue line*), we see that the signal stretches out 5 zones, reflecting evenly across each zones partition back to the original power in *black dotted*

where N is the number of samples used.

The reduction from FT to DFT comes with consequences such as introducing a finite frequency resolution. We have broken our signal into discrete time samples, introducing intervals of finite width, meaning that frequencies too close together will appear as just one.

The bandwidth of possible frequencies resolved by a DFT ranges from $[-\nu_N, \nu_N]$, where the negative frequencies imply a phase shift of $\pi/2\, radian$ and represent the cosine components. The frequency resolution then is the division of this bandwidth by the number of samples used, N, and can be written as.

$$\Delta\nu_{min} = \frac{v_s}{N} \tag{6}$$

We test this by combining $10\, MHz$ and $10\, MHz + \Delta\nu\, MHz$ and and find frequencies separated by less than $\Delta\nu = .003\, MHz$ are unable to be resolved, i.e. one cannot tell that there are two 'spikes.' We would expect to find a frequency resolution of $\sim 1.98\, kHz$ when sampling with 15800 points at a frequency of $v_s = 31.25$ but we found the minimum resolvable frequency was almost 2 times this at $3\, kHz$.

Now that we have our data in the frequency domain we can understand why we saw the reflection of periods about the Nyquist frequency. Our functions in the frequency domain are made up of complex sine functions which map a circle in the complex plane. Our bandwidth of $[-\nu_s/2, \nu_s/2]$ is not describing a closed section on a line, but a circle that continuously wraps around. This is to say, when we sample higher than the Nyquist frequency, we are measuring greater than a rotation around the circle but still providing a frequency existing in the circle. This periodic symmetry gives rise to Frequency Windows which reflect about multiples of the Nyquist frequency, symmetrically falling back onto the original bandwidth.

To test for this effect, we compute the power spectrum over larger bandwidths than $[-\nu_s/2, \nu_s/2]$ for a non-aliased signal. In figure 3 we see the cascading aliasing effect of our power spectrum through reflections over integer multiples of the Nyquist frequency finally landing inside our original bandwidth. Each Nyquist 'zone,' is represented in a different color to make clear this effect.

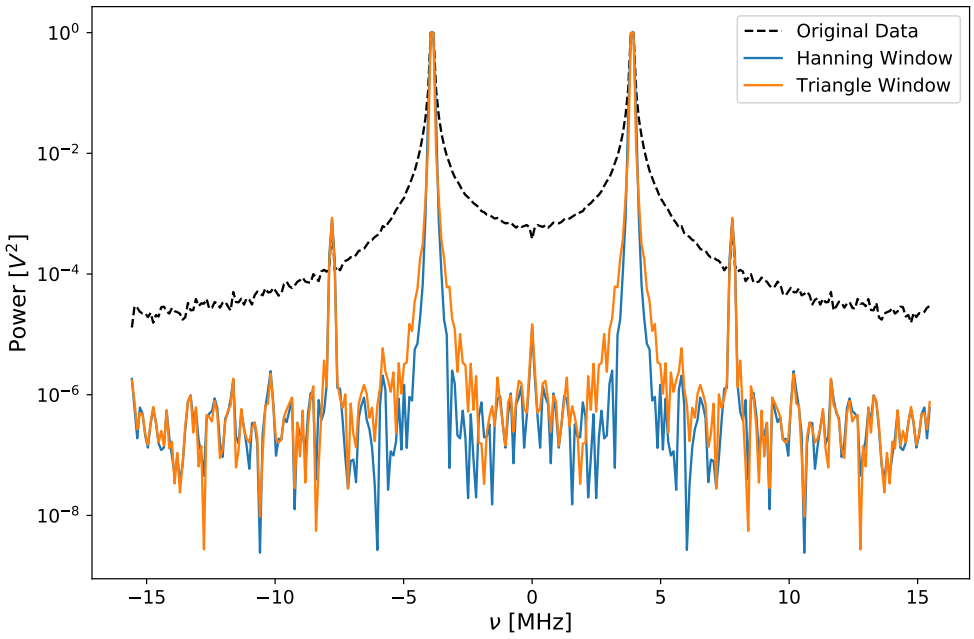

Figure 4: As an example of frequency leakage we plot the power spectrum for a 3.125 MHz sine wave, *black dashed*, which has essentially been multiplied by a boxcar filter causing spectral leakage. We compare this with windows of equal length, but varying shape on the same signal to show the effect of reducing the power in neighboring frequencies by $\tilde{4}$ orders of magnitude thus reducing spectral leakage. In reducing the power in the side-lobes of the *sinc* function caused by the Fourier transform of the boxcar filter, we resolve a more accurate power spectra but sacrifice frequency resolution.

3.3 Convolution and Auto Correlation

We have seen some of the impacts from discretizing our sampling and to further understand how this impacts our analysis, we need to consider the convolution, or multiplication, of signals. The theorem states that,

$$\begin{aligned}[F * G](\tau) &= \int_{-T/2}^{T/2} F(t)G(\tau - t)dt \\ \widetilde{[F * G]}(\tau) &= \int_{-T/2}^{T/2} [F * G]e^{2\pi i \tau \nu} d\tau = \widetilde{F}(\nu) \times \widetilde{G}(\nu)\end{aligned} \tag{7}$$

where τ is delay and represents the sliding of G across F, smoothing it with time. From the moment we sample a convolution in time has restricted our infinite signal to a 'box' with a width equal to the length of time range of samples. This can be described as convolving our function with a 'boxcar filter' defined as,

$$W_{B.C}(t) = \begin{cases} 1 & \text{For } 0 \leq t \leq N\Delta t \\ 0 & \text{For } 0 > t \text{ and } t > N\Delta t \end{cases}. \tag{8}$$

Because the FT of a boxcar is a function (as $sinc(x) = \sin(x)/x$), and the fourier transform of a sine wave is a delta function, our signal spreads power over the shape of a *sinc* about the peak of the sine wave delta functions. The black dashed line of figure 4 shows this effect, where the power of our data is broadened to non zero frequencies across the entire bandwidth. We use alternate convolutions in fig 4, to show the effect of alternate convolutions by windowing functions. We use both a *Hanning* (eq 9) and *Triangle* (eq 10) function to see the resulting power spectra.

$$W_T(t) = \begin{cases} .5\left(1 - \cos\left(2/N\right)\right) & \text{For } 0 \leq t \leq N\Delta t \\ 0 & \text{For } 0 > t \text{ and } t > N\Delta t \end{cases} \tag{9}$$

$$W_H(t) = \begin{cases} 2t/N & \text{For } 0 \leq t \leq N\Delta t/2 \\ 2 - 2t/N & \text{For } N\Delta t/2 \leq t \leq N\Delta t \\ 0 & \text{For } 0 > t \text{ and } t > N\Delta t \end{cases} \tag{10}$$

Figure 4, shows that the window functions limit the amount of spectral leakage by ~ 2 orders of magnitude allowing for a more accurate spectral reconstruction. Though the resolution is enhanced, there is also a decrease in the frequency resolution because of the uneven weighting to individual samples through out the data.

The Correlation Theorem is similar to the convolution theorem but determines the amount by which a signal is related to another. It is defined as,

$$\begin{aligned} [F \star G](\tau) &= \int_{-T/2}^{T/2} F(t)G(\tau + t)dt \\ \widetilde{[F \star G]}(\tau) &= \int_{-T/2}^{T/2} [F \star G](\tau)e^{2\pi i\nu\tau}d\tau = \widetilde{F}(\nu) \times \widetilde{G}^*(\nu) \end{aligned} \tag{11}$$

This can be visualized by sliding one function across another and marking how similar the functions are against how much you had to slide one function to find the similarity.

We find a relationship with Energy when correlating a function with its self (auto-correlating). Because our signals are functions of time, this becomes a representation of the power in the time domain and we can find the power we previously explored in the frequency domain by Fourier transforming the auto-correlation function.

$$\begin{aligned} ACF(\tau) &= [F \star F](\tau) \\ \widetilde{ACF}(\nu) &= \widetilde{F}(\nu) \times \widetilde{F}^*(\nu) = |\widetilde{F}|^2 = \widetilde{P}(\nu) \end{aligned} \tag{12}$$

4 Interpretation

In this section we use the analysis from above and consider practical applications of these methods. We first apply our knowledge of FT's to Gaussian noise to explore how averaging can reduce spectral variation in noise. We then conclude with a comparison of ideal and realistic mixers giving some brief examples of when they are used in astronomy.

4.1 An Application: Noise

Noise is characterized by temperatures of an observing system, such as an antenna, and the source being observed, such as a black-body. Noise and power are related to temperature and therefore inherently related to each other. Here we explore random Gaussian noise and show that taking multiple samples allow us to coherently average and decrease the variance in the power.

We average the signals by first sampling 32 blocks of the Gaussian noise with 15800 samples per block. We then compute the power spectrum of each block and average over 2^B blocks with $B = [0, 5]$. Figure 5 shows the power spectra of the averaged blocks. After this averaging we calculate the variance of the power over a frequency range of $[9.765\,MHz, 10.953\,MHz]$. In this calculation we find a decrease in the variance by $\sim 86\%$ (table **??**). —r—r—

4.2 Mixers

In this section we use the concepts of correlation and convolution to explore mixers. Mixers multiply signals of varying frequencies together making a new waveform with a different frequency. We test two different types of mixers, single side-band and double side-band, as well as the effect of filtering.

For both single and double side-band mixers, (SSB, DSB) we multiply a local oscillator (LO) with a radio frequency (RF) to obtain an intermediate frequency (IF) which is inside of the nyquist criterion. The

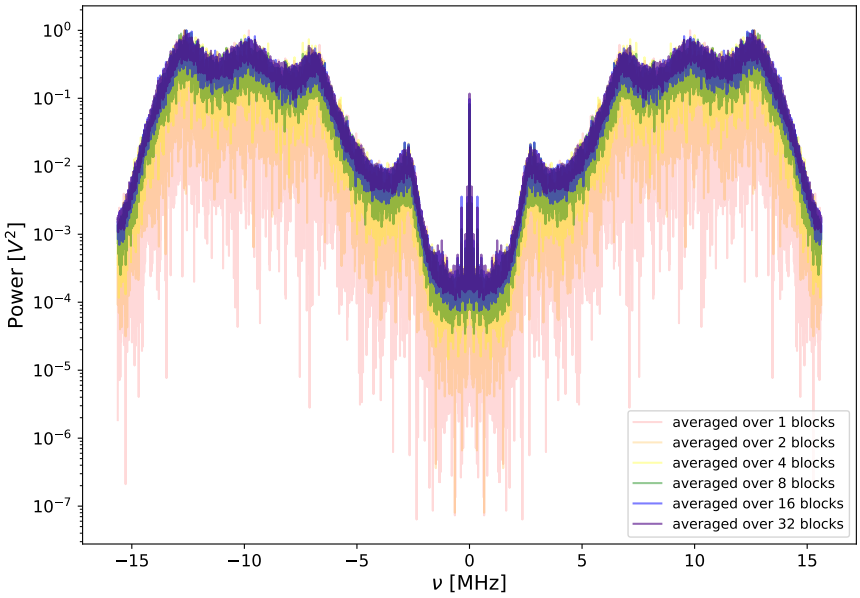

Figure 5: We show the effect of coherent averaging for random Gaussian noise with no attenuation. The power spectrum gradually sharpens as we increase the number of blocks we sample over, decreasing the variance of the power.

Blocks of Averaging	Variance, σ
1	1.6686
2	0.959768
4	0.492706
8	0.308001
16	0.264533
32	0.23714

Table 1: We accompany figure 5 with the values of the variance as the power is averaged over increasing blocks of 16000 samples resulting in an 86% decrease

difference between a SSB and DSB is the resulting intermediate frequency's obtained. For a SSB, when we introduce a 90 degree phase shift between both mixers, we find that the real and introduced imaginary components individually contain a side-band. For the DSB, the information of the side bands is mixed into one signal and we cannot extract the side bands individually.

We illustrate this difference by first providing the mathematical theory of why this is the case and then by showing evidence from experimentation.

The SSB is more complex of a setup than the DSB because it is multiplying the RF by two functions separated by a $\pi/2$ phase shift. We can use Euler's Identity to write this voltage as

$$V_{LO,SSB} = e^{-i\omega_{LO}t} = \cos(\omega_{LO}t) - i\sin(\omega_{LO}t) \tag{13}$$

Where $-\omega_L O$ represents the angular frequency of the LO, which has a $\pi/2$ phase shift. For the DSB, there is no complex component or phase, the LO is simply a sine wave,

$$V_{LO,DSB} = \sin(\omega_{LO}t) \tag{14}$$

In both cases we multiply the LO by a RF which is defined as,

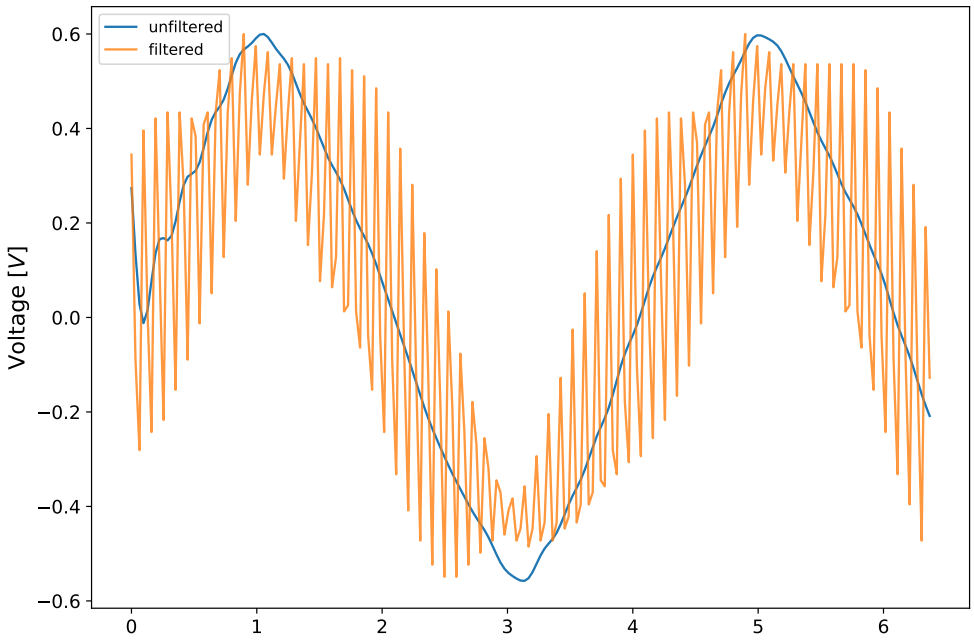

Figure 6: We show the effects applying a boxcar filter with a width of 18 MHz, centered at $\nu = 0$ on a signal mixed with $\nu_{LO} = 10\,MHz$ and $\Delta\nu = \pm.5\,kHz$ to a double side-band mixer. The *orange lines* represent the unfiltered signal and the *blue lines* the filtered. This process smooths our signal in its voltage (*Top Panel*). Mixers are working to bring a high frequency to a radio frequency, so it makes sense that would want to apply a filter and achieve these results.

$$V_{RF} = V_A \sin(\omega_{LO} \pm \Delta\omega) \tag{15}$$

Where for $\Delta\omega$ we have chosen a value 5% above our LO so that, $\Delta\omega = .05\omega_{LO}$. Multiplying both the DSB and SSB voltages with V_{RF} the result leads to,

$$\begin{aligned} V_{IF,SSB} &= \frac{V_A}{2i}\left[e^{\pm i\Delta\omega t} - e^{-i(2\omega_{LO}\pm\Delta\omega)}\right] \\ V_{IF,DSB} &= V_A\left[\cos(\pm\Delta\omega t) - \cos\left(2\omega_{LO} \pm \Delta\omega\right)\right] \end{aligned} \tag{16}$$

Because we are usually only interested in the low frequency outputs of these waves, the important difference in these equations is the beat frequencies,

$$\begin{aligned} V_{beat,SSB} &= \frac{1}{2}\left[V_A(\pm\sin(\Delta\omega t) + i\cos(\Delta\omega t))\right] \\ V_{beat,DSB} &= V_A\cos(\Delta\omega t) \end{aligned} \tag{17}$$

We see from equation 17, that the $\pm$ in front of the sine wave allow single side-band mixers to differentiate between RF frequencies. The DSB cannot because it does not contain the complex component present in the SSB.

We test the above theories with a LO set to $\nu_{LO} = 10\,MHz$, $\Delta\nu = .5\,MHz$ and $\nu_{RF} = 10\,MHz \pm .5\,MHz$. Calculating the power spectra for both ν_{RF}'s independently and applying a boxcar to the DSB data (6) to remove frequencies above $9\,MHz$ we resolve the beat frequencies which exist at $\pm 5\,MHz$.

In figure 7 we plot the power spectra of V_{IF} using both ν_{RF}'s for each mixer. The top plot shows a filtered power spectrum of the DSB, while the bottom two show a SSB with and without a $pi/2$ phase shift. What becomes clear is that while all plots show a peak at $\Delta\nu$ as we would expect, only the last plot, where the SSB contains a $\pi/2$ phase shift between the LO and one mixer, is there a clear delineation between the side bands. This verifies our math shown above and provides useful insight into optimal mixing. While it is cheaper (only costs one mixer) to build a DSB, it removes our ability to differentiate between side-bands providing less information to be analyzed.

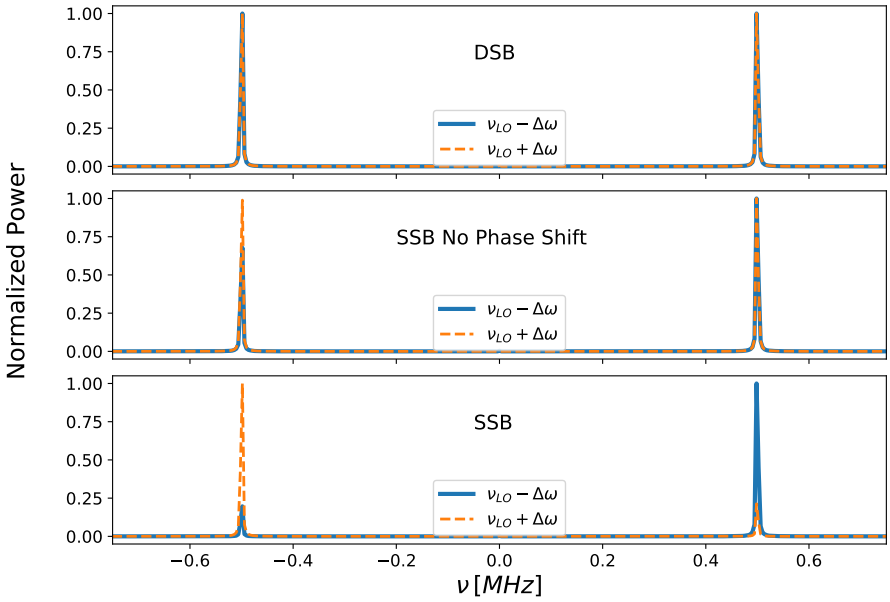

Figure 7: We show the power spectra of the IF outputs for DSB (*Top Plot*), and SSB mixers (*Bottom Plots*). We use an $\nu_{RF} = 10\,MHz \pm .5\,Mhz$ and $\nu_{LO} = 10\,MHz$. The only plot that shows a dilineation between the two input signals is the SSB that contains a phase shift. This is seen in the two RF's having different power spectra, one in only the negative $\Delta\nu$ (*Orange Dashed*) while the other only has positive $\Delta\nu$ (*Blue*)

5 Conclusion

Through this work we have discussed and verified many of the fundamental components for radio astronomy: How to sample and how fast to sample a signal, how to analyze a signal in the frequency domain, possible pitfalls, how to average noise and how to multiply signals. Combining these components is the essence of radio astronomy and are considerations likely taken by Grote Reber in 1937 during his first radio observations. Though we scratch the surface, the hope is that enough information and evidence has been provided to give a frame work for radio signal processing and analysis as a whole.

6 Acknowledgments

I worked with most of the scripting for taking the data, and helped set up some of the experiments, Connor and James did a majority of setting the equiptment up and Basil provided insight into the math and theory.